
LEVEL THREE SYNTHETIC FINGERPRINT GENERATION

A PREPRINT

André Brasil Vieira Wyzykowski, Mauricio Pamplona Segundo, Rubisley de Paula Lemes *
Intelligent Vision Research Lab
Federal University of Bahia, Brazil

February 11, 2020

ABSTRACT

Today’s legal restrictions that protect the privacy of biometric data are hampering fingerprint recognition researches. For instance, all public databases of high-resolution fingerprints ceased to be publicly available. To address this problem, we present an approach to creating high-resolution synthetic fingerprints. We modified a state-of-the-art fingerprint generator to create ridge maps with sweat pores and trained a CycleGAN to transform these maps into realistic prints. We also create a synthetic database of high-resolution fingerprints using the proposed approach to propel further studies in this field without raising any legal issues. We test this database with two existing fingerprint matchers without adjustments to confirm the realism of the generated images. Besides, we provide a visual analysis that highlights the quality of our results compared to the state-of-the-art.

Keywords Synthetic fingerprints · Level-3 features · CycleGAN · PolyU HRF database.

1 Introduction

Fingerprint recognition is widely studied thanks to its compliance with the core premises of biometrics: permanence and distinctiveness [1, 2]. Patterns on fingerprint images can be analyzed at different scales and resolutions. These patterns can be classified as Level 1 (L1 - global patterns, such as ridge orientation maps, and fingerprint classes), Level 2 (L2 - local patterns, such as minutiae) and Level 3 (L3 - fine details, such as sweat pores, incipient ridges and dots).

With the development of high-resolution sensors able to capture L3 fingerprint images, researchers saw an opportunity to devise new and more accurate recognition approaches by using the most exploited L3 feature in the literature, the presence of sweat pores [3, 4, 5]. Besides, L3-based approaches improve security by hindering spoof attempts [6, 7, 8].

Despite the recent improvements brought to the fingerprint recognition research area, L3 fingerprint databases are being discontinued. For instance, databases such as the NIST Special Database 30 [9] and the Hong Kong Polytechnic University High Resolution Fingerprint database (PolyU) [10] are no longer publicly available. More recently, Anand and Kanhangad [11, 12] created L3 databases for their recognition experiments. However, until the present moment, these databases were not released. The main reason for that is the existence of legal restrictions that protect the privacy of biometric data, which hinders the evolution of fingerprint recognition research.

To tackle this problem, as our main contribution, we present a novel approach to create realistic, high-resolution synthetic fingerprints (see Section 2). With that, we also create an L3 synthetic database² (see Section 3). Our main goal is to motivate further studies in this field without raising legal issues that come with real biometric data.

SFinGe [13] and Finger-GAN [14] are also capable of generating synthetic fingerprints. However, they have some limitations. SFinGe restricts the generation of large datasets and does not create realistic L3 traits. Finger-GAN

*This research was funded by CNPq (<http://cnpq.br/>). The Titan Xp used for this research was donated by the NVIDIA Corporation.

²<https://andrewyzy.github.io/L3-SF/>

images are not realistic and do not contain pores. The proposed approach outperformed both SFinGe and Finger-GAN in a visual comparison (see Section 4).

2 SYNTHETIC FINGERPRINT GENERATION

To generate high resolution synthetic fingerprints, we split our approach into two stages. The first stage concerns the master fingerprint creation and other procedures required to create multiple instances of these fingerprints, which we call seed images. The second stage consists of using CycleGAN [15] to translate seed images into realistic L3 fingerprints. Figure 1 summarizes the workflow required to create a high-resolution synthetic fingerprint.

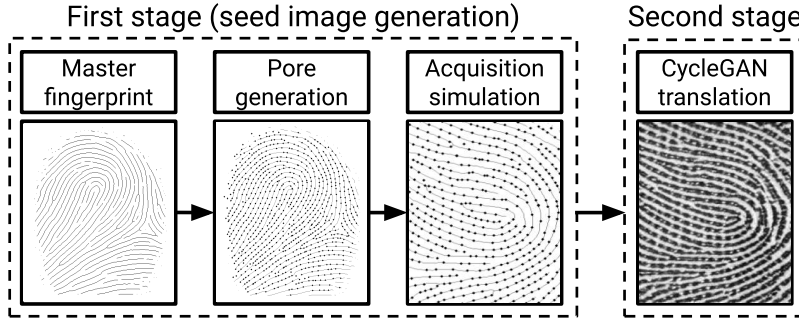


Figure 1: Steps to create a high-resolution synthetic fingerprint.

The first stage consists of the following processes:

1. **Master fingerprint generation:** we use Anguli [16], an open-source implementation of SFinGe [13], to create fingerprint ridge maps with random ridge-flow patterns and without texture and noise variations. After skeletonization, these images are called master fingerprints (see Section 2.1).
2. **Pore generation:** we add pores to each master fingerprint following a pore distribution learned from real images. We call the resulting images L3 master fingerprints (see Section 2.2).
3. **Fingerprint acquisition simulation:** to simulate acquisition, we randomly cut the L3 master fingerprints following a distribution of the displacement among images of the same person in a real database, thus creating different instances for each identity. These instances are called seed images (see Section 2.3).

The second stage consists of the following processes:

1. **Training set generation:** to train a CycleGAN, we use several seed images created by the first stage of our approach and a database of real high-resolution fingerprints. To reduce the gap between them, we also transform real fingerprints into seed images through binarization, skeletonization and pore generation (see Section 2.4). Finally, data augmentation is applied to real images and their seed versions (see Figure 6).
2. **CycleGAN training:** uses the training set to create a CNN model that translates seed images to high-resolution fingerprints (see Section 2.5).
3. **CycleGAN inference:** transforms any seed image into a realistic L3 fingerprint (see Figure 7).

2.1 Master fingerprint generation

We use Anguli [16] to create the ridges map that compose a master fingerprint within one of the following classes: Whorl, Right Loop, Left Loop, Plain Arch, and Tented Arch. Examples of these classes are shown in Figure 2.

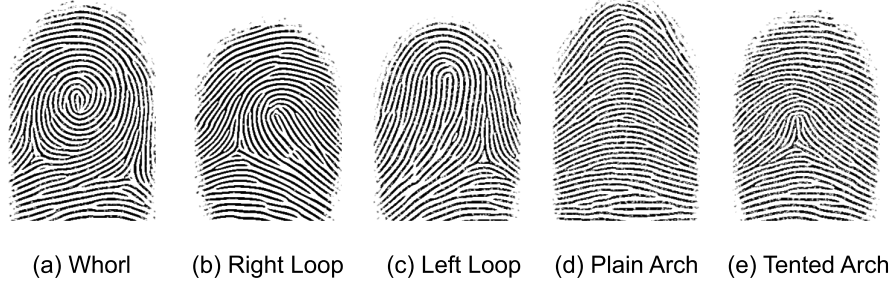


Figure 2: Five fingerprint class patterns created by Anguli.

These ridges maps are then skeletonized using Zhang-Suen’s thinning algorithm [17] to create master fingerprints.

2.2 Pore generation

This step consists in marking where the pores will be placed on the skeletonized ridges. To measure and apply the distance distribution from one pore to another, we use a pore-based ridge reconstruction approach [3]. Given a training set of real fingerprint images, we compute the average distance and the standard deviation between neighboring pores. We then sample from this distribution using the normal inverse cumulative distribution function.

Starting from the beginning of a ridge, we iteratively generate distances d_i using the above distribution. We follow the ridge pixels to add the i -th pore d_i away from the previous pore until the end of the ridge is reached. This process to create L3 master fingerprints is illustrated in Figure 3.

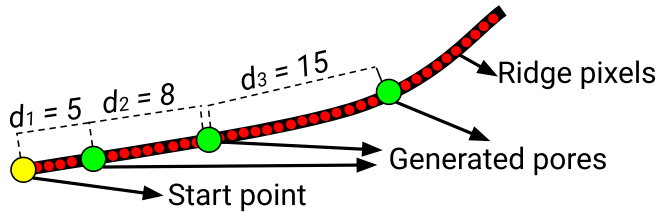


Figure 3: Illustration of the pore generation process. Red circles represent a sequence of pixels in a ridge and the green circles are the generated pores. Given a start point, pore distances are sampled using the normal inverse cumulative distribution function. In this example, new pores are created with distances $d_1 = 5$, $d_2 = 8$ and $d_3 = 15$.

2.3 Fingerprint acquisition simulation

Different finger positions on the image sensor produce distinct rotations and shifts on fingerprint images. Our approach aims to simulate these acquisition variations.

To measure rotation and shift variations between fingerprints of the same person from a training set, we extract SIFT keypoints [18, 19], establish correspondences, and use the RANSAC algorithm [20] to estimate the transformation parameters. We then calculate the mean and standard deviation of rotation and translation values for the entire training set.

To create a seed image, we sample a random transformation from the above distribution using the normal inverse cumulative distribution function. After that, we use the obtained values to rotate and translate the L3 master fingerprint before cropping the center region of the resulting image. Examples of seed images from the same L3 master fingerprint are shown in Figure 4.

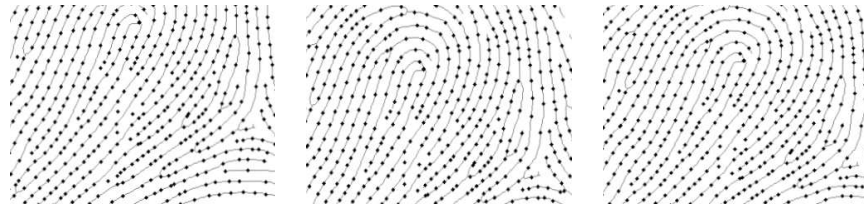


Figure 4: Seed images generated from a single L3 master fingerprint, presenting distinct shifts and rotations.

2.4 Seed images from real images

In order to reduce the gap between synthetic seed images and real fingerprints, we transform the latter into seed images as well. To this end, we applied the following sequence of operations: histogram equalization using CLAHE [21], mean filtering, Otsu’s binarization [22], Zhang-Suen’s thinning [17], and pore generation (as in Section 2.2). A diagram of this process is shown in Figure 5.

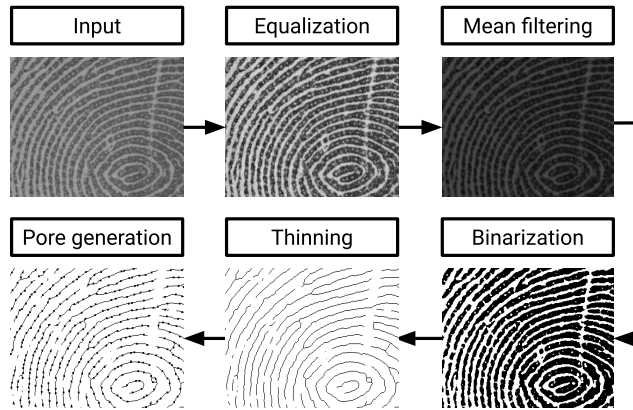


Figure 5: Steps to create seed images from real fingerprints.

Even though pores in the resulting seed image are not aligned with the pores in the respective real image, this is not a problem because CycleGAN does not require paired structures to map and translate image domains.

2.5 CycleGAN-based domain translation

To generate realistic fingerprint images, we learn to map the seed image domain into the real image domain of the chosen training database using CycleGAN [15].

CycleGAN is viable solution for the task of translating two different domains as it does not require direct pairing between their training instances. Thus, our seed images do not need to be perfectly aligned to a real image in the training set.

To increase the number of training images, we apply elastic deformations through random affine transformations [23] to real and seed images. Figure 6 exemplifies this process.

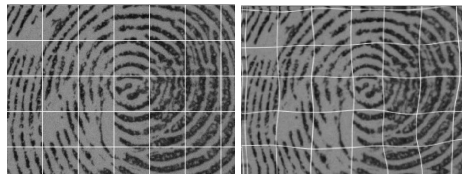


Figure 6: Real fingerprint (left) and its augmented version (right). White lines highlight the applied transformation.

After that, we are able to translate any seed image into a realistic fingerprint. Examples of the inference using CycleGAN are presented in Figure 7.

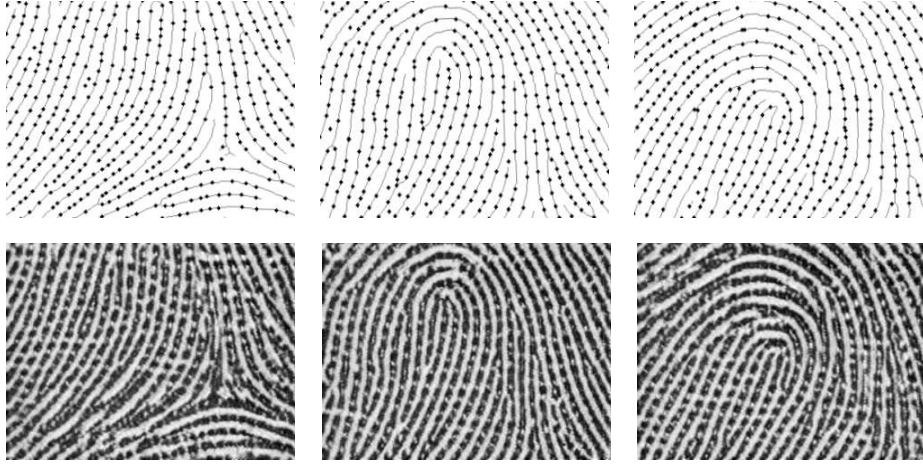


Figure 7: CycleGAN inference: seed images (top) and their respective results (bottom).

3 SYNTHETIC DATABASE CREATION

Knowing that Anguli produces five fingerprints classes, it was necessary to determine the proportion of these classes in a real population. Martijn van Mensvoort [24] gathered fingerprint distributions from 32 countries through a compilation of 28 published articles. Each country has its peculiarities and proportions, so we decided to use the global mean distribution.

The mean distribution for 32 countries is: Whorl: 41%, Right Loop: 50%, Left Loop: 3%, Arch: 6%. Since Anguli can create two arch fingerprint types (plain or tented arch), we used the ratio provided by Wang [25]: Plain Arch: 72.22% and Tented Arch: 27.77%. Following this distribution, we create 600 L3 master fingerprints for training.

When simulating fingerprint acquisition, we used the structure of the DBI subset of the PolyU database: two acquisition sessions, each containing five images per person. Thus, we end up with 6000 seed images with 320×240 pixels.

We perform data augmentation on PolyU DBI images and their seed versions, totaling 2960 real fingerprints and 2960 additional seed images of 320×240 pixels for training. Then, all these nearly 12000 images are the input to the CycleGAN training. The last step consists of inferring 1480 seed images from 148 identities using the obtained CycleGAN model to obtain a synthetic database with the same structure of PolyU DBI. This group of images composes our L3 synthetic fingerprint (L3-SF) database.

4 Experiments and Results

The goal of this experiment is to compare the behavior of real and synthetic images in terms of recognition performance. Ideally, both should have close results. To carry out this comparison, first we utilize Bozorth3 [26], which is a minutia-based fingerprint matching approach. To perform pore-based fingerprint matching, we utilize Segundo and Lemes' approach [3]. To perform this analyses, we use the same protocol proposed by Liu et al. [27] for PolyU DBI and L3-SF, as both databases have the exact same configuration (i.e. number of images per person, number of sessions, number of subjects and image size).

We computed the False Rejection Rate (FRR) and the False Acceptance Rate (FAR) using different threshold values for both matching approaches. The obtained FRR and FAR are shown as a Receiver Operating Characteristic (ROC) curve in Figure 8.

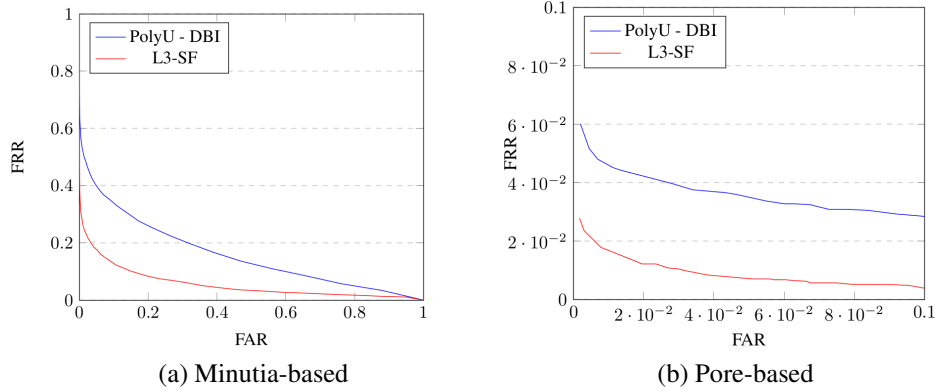


Figure 8: ROC curves for (a) minutia-based and (b) pore-based matching approaches using PolyU and L3-SF databases.

The Equal Error Rate (EER) values for minutia-based matching are 23.84% for real images and 11.83% for synthetic ones. The EER values for pore-based matching are 3.37% for real images and 1.43% for synthetic ones. A possible cause of this difference in performance is the lack of non-linear deformations in the acquisition simulation, where we seek to reduce this difference by simulating deformations in future versions of our synthetic fingerprint generator, because one of our goals is to create a synthetic dataset as challenging as a real one for recognition. Still, these results validate L3-SF images as realistic fingerprints, as existing recognition methods were successful without any adjustments.

A visual comparison of real and our synthetic fingerprints is shown in Figure 9. Note that synthetic images have a similar style while real images are very different from each other. This may be one of the reasons why the recognition performance is higher for synthetic images, and is one of the challenges to be addressed in the future.

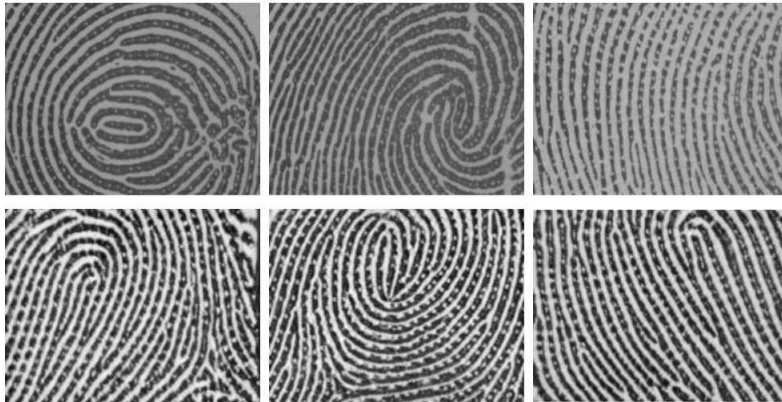


Figure 9: Visual comparison between real fingerprints from PolyU DBI (top) and synthetic ones from L3-SF (bottom).

Even so, L3-SF fingerprints contain different realistic aspects, such as having pores with different sizes and shapes, and showing texture details in ridges. Meanwhile, SFinGe [13] generates rectangular, single-sized pores and FingerGAN [14] does not generate pores at all. Besides, FingerGAN produces unnatural ridge shapes while SFinGe produces different unrealistic patterns in ridges, such as edges with a staircase appearance. Figure 10 shows a visual comparison between fingerprints generated by the proposed approach, by a publicly available SFinGe demo, and by our own implementation of FingerGAN.

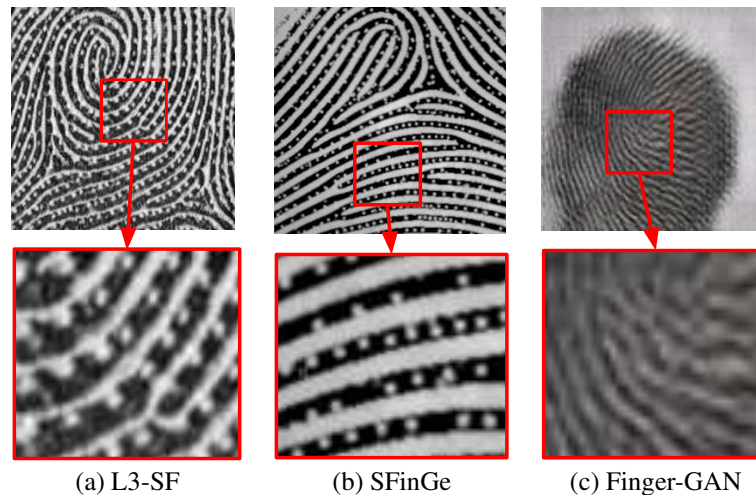


Figure 10: Visual comparison between (a) the proposed approach, (b) SFinGe, and (c) Finger-GAN.

5 Conclusions

We present an approach to generate realistic, high-resolution synthetic fingerprints containing pore information on the ridges. We trained a CycleGAN using real fingerprint images from PolyU and seed images to create a model capable of translating between these two image domains. Using this model, we created the L3-SF database with the same characteristics of the PolyU DBI. Our experimental results show that L3-SF images can be used by existing fingerprint recognition methods without any adjustments. Finally, a visual comparison highlights the improvements in terms of realism when the proposed approach is compared to the state-of-the-art.

Our methodology and dataset allow further studies in the field of fingerprint biometrics without raising privacy-related legal issues. Still, there is a margin for improvements in our synthetic fingerprint generator, because synthetic images should be as challenging as real images for recognition. In future works, we intend to add non-linear deformations to seed images in the acquisition simulation, and to increase variations in style using other architectures, such as MUNIT [28].

References

- [1] D. Maltoni, D. Maio, A. K. Jain, and S. Prabhakar. *Handbook of Fingerprint Recognition*. Springer London, 2009.
- [2] A. K. Jain and A. Kumar. Biometrics of next generation: An overview. *Second Generation Biometrics*, 12(1):2–3, 2010.
- [3] M. Pamplona Segundo and R. de Paula Lemes. Pore-based ridge reconstruction for fingerprint recognition. In *2015 IEEE Conference on Computer Vision and Pattern Recognition Workshops*, pages 128–133, June 2015.
- [4] V. Anand and V. Kanhangad. Porennet: Cnn-based pore descriptor for high-resolution fingerprint recognition. *CoRR*, abs/1905.06981, 2019.
- [5] D. Nguyen and Anil K. Jain. End-to-end pore extraction and matching in latent fingerprints: Going beyond minutiae. *CoRR*, abs/1905.11472, 2019.
- [6] M. Espinoza and C. Champod. Using the number of pores on fingerprint images to detect spoofing attacks. *2011 International Conference on Hand-Based Biometrics, ICHB 2011 - Proceedings*, Nov 2011.
- [7] G. L. Marcialis, F. Roli, and A. Tidu. Analysis of fingerprint pores for vitality detection. In *2010 20th International Conference on Pattern Recognition*, pages 1289–1292, Aug 2010.
- [8] M. da Silva, A. Marana, and A. Paulino. On the importance of using high resolution images, third level features and sequence of images for fingerprint spoof detection. In *IEEE International Conference on Acoustics, Speech and Signal Processing*, pages 1807–1811, Apr 2015.
- [9] "National Institute of Standards and Technology". Nist special database 30. <https://www.nist.gov/srd/nist-special-database-30>, 2002.

- [10] Q. Zhao, L. Zhang, D. Zhang, and N. Luo. Direct pore matching for fingerprint recognition. In Massimo Tistarelli and Mark S. Nixon, editors, *Advances in Biometrics*, pages 597–606. Springer Berlin Heidelberg, 2009.
- [11] V. Anand and V. Kanhangad. Cross-sensor pore detection in high-resolution fingerprint images using unsupervised domain adaptation. *arXiv preprint arXiv:1908.10701*, 2019.
- [12] V. Anand and V. Kanhangad. Pore-based indexing for fingerprints acquired using high-resolution sensors. *Pattern Analysis and Applications*, Mar 2019.
- [13] R. Cappelli. Sfinge: an approach to synthetic fingerprint generation. *International Workshop on Biometric Technologies*, Jan 2004.
- [14] S. Minaee and A. Abdolrashidi. Finger-gan: Generating realistic fingerprint images using connectivity imposed gan. *arXiv preprint arXiv:1812.10482*, 2018.
- [15] J. Zhu, T. Park, P. Isola, and A. A. Efros. Unpaired image-to-image translation using cycle-consistent adversarial networks. *CoRR*, abs/1703.10593, 2017.
- [16] A. H. Ansari. Generation and storage of large synthetic fingerprint database. *ME Thesis, Jul*, 2011.
- [17] T. Y. Zhang and C. Y. Suen. A fast parallel algorithm for thinning digital patterns. *Commun. ACM*, 27(3):236–239, March 1984.
- [18] D. G. Lowe. Object recognition from local scale-invariant features. In *Proceedings of the International Conference on Computer Vision-Volume 2 - Volume 2, ICCV '99*, pages 1150–, Washington, DC, USA, 1999. IEEE Computer Society.
- [19] D. G. Lowe. Distinctive image features from scale-invariant keypoints. *International Journal of Computer Vision*, 60(2):91–110, 2004.
- [20] M. A. Fischler and R. C. Bolles. Random sample consensus: A paradigm for model fitting with applications to image analysis and automated cartography. *Commun. ACM*, 24(6):381–395, June 1981.
- [21] K. Zuiderveld. Graphics gems iv. chapter Contrast Limited Adaptive Histogram Equalization, pages 474–485. Academic Press Professional, Inc., San Diego, CA, USA, 1994.
- [22] N. Otsu. A threshold selection method from gray-level histograms. *IEEE Transactions on Systems, Man, and Cybernetics*, 9(1):62–66, Jan 1979.
- [23] P. Y. Simard, D. Steinkraus, J. C. PLATT, et al. Best practices for convolutional neural networks applied to visual document analysis. In *Seventh International Conference on Document Analysis and Recognition, 2003. Proceedings.*, pages 958–963, Aug 2003.
- [24] M. van Mensvoort. The fingerprints-world-map! <http://fingerprints.handresearch.com/dermatoglyphics/fingerprints-world-map-whorls-loops-arches.htm>, mar 2015.
- [25] Patrick S. P. Wang, editor. *Pattern Recognition, Machine Intelligence and Biometrics*. Springer Berlin Heidelberg, 2011.
- [26] "National Institute of Standards and Technology". Nist biometric image software (nbis). <https://www.nist.gov/services-resources/software/nist-biometric-image-software-nbis>, 2015.
- [27] F. Liu, Q. Zhao, L. Zhang, and D. Zhang. Fingerprint pore matching based on sparse representation. *2010 20th International Conference on Pattern Recognition*, pages 1630–1633, 2010.
- [28] X. Huang, M. Liu, S. J. Belongie, and J. Kautz. Multimodal unsupervised image-to-image translation. *CoRR*, abs/1804.04732, 2018.